Joule

CellPress

Article

Designing a Quinone-Based Redox Mediator to Facilitate Li_2S Oxidation in Li-S Batteries

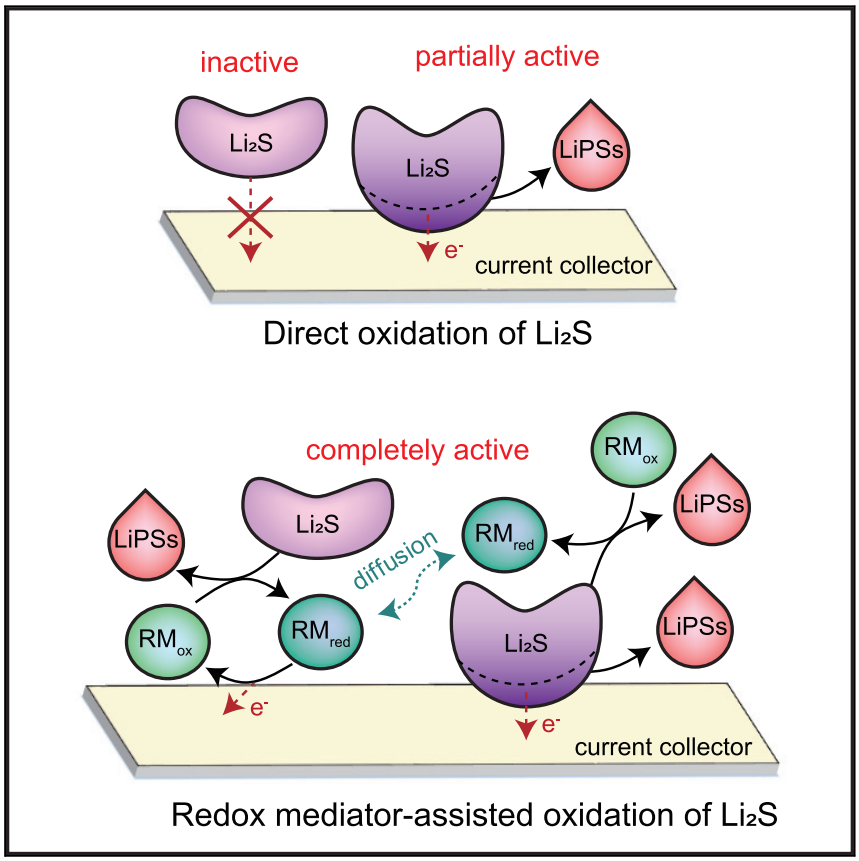

We utilized quinone redox chemistry to design a new RM for fast and stable cycling of Li-S batteries. Through rational tuning of the redox potential, stability, and solubility of quinones by molecular engineering, we successfully demonstrated that the quinone redox can facilitate the Li_2S oxidation and the maintained Li_2S original morphology. The introduction of AQT as an RM is a simple and effective approach to significantly enhance multiple aspects of sulfur redox chemistry under challenging conditions.

Yuchi Tsao, Minah Lee, Elizabeth C. Miller, ..., Michael F. Toney, Yi Cui, Zhenan Bao

yicui@stanford.edu (Y.C.)
zbao@stanford.edu (Z.B.)

HIGHLIGHTS

The redox chemistry of a quinone derivative is employed to facilitate Li_2S oxidation

Tailoring redox potential, solubility, and stability of quinone enhances performance

Initial charging of Li_2S < 2.5 V at a 0.5C rate is achieved with the tailored quinone

Deposition of dead Li_2S is prevented with quinone enabling longer cycle life

Tsao et al., Joule 3, 872–884
March 20, 2019
https://doi.org/10.1016/j.joule.2018.12.018

Joule

CellPress

Article

Designing a Quinone-Based Redox Mediator to Facilitate Li_2S Oxidation in Li-S Batteries

Yuchi Tsao,[1,7] Minah Lee,[2,7] Elizabeth C. Miller,[3] Guoping Gao,[4] Jihye Park,[2] Shucheng Chen,[2] Toru Katsumata,[2,5] Helen Tran,[2] Lin-Wang Wang,[4] Michael F. Toney,[3] Yi Cui,[6,*] and Zhenan Bao[2,8,*]

SUMMARY

In lithium-sulfur (Li-S) batteries, the insulating nature of sulfur and lithium sulfide (Li_2S) results in large polarization and low sulfur utilization while the soluble polysulfides lead to internal shuttle upon cycling. Furthermore, the redox reaction via the dissolution-precipitation route destroys the electrode architecture by passivating the active interface responsible for the redox reaction, and thus the performance deteriorates with cycling. Here, we employ the redox chemistry of quinone to realize efficient, fast, and stable operation of Li-S batteries using Li_2S microparticles. By adding a quinone derivative with tailored properties (e.g., oxidation potential, solubility, and electrochemical stability) to an electrolyte as a redox mediator (RM), initial charging of Li_2S electrodes occurs below 2.5 V at 0.5C, and the subsequent discharge capacity is as high as 1,300 mAh g_s^{-1}. Moreover, deposition of dead Li_2S, which was the primary cause of increasing polarization and decreasing capacity upon cycling, is effectively prevented with the RM.

INTRODUCTION

Lithium-sulfur (Li-S) batteries are a sustainable and cost-effective solution for next-generation energy storage to support renewable energy integration due to the natural abundance of sulfur.[1,2] Li-S batteries can theoretically store an energy density of 2,500 Wh kg^{-1}, a 5-fold increase compared to traditional lithium ion batteries (LIBs).[3] Such exceptionally high energy density is enabled by the reversible conversion reaction between sulfur and lithium sulfide (Li_2S) via a series of lithium polysulfides intermediates (LiPSs, Li_2S_n, $2 \leq n \leq 8$).[4] However, significant challenges remain in order to build practical Li-S batteries, which are mainly attributed to the solubility of LiPSs in the electrolytes and the insulating nature of both sulfur and Li_2S.[5,6] For example, when charging a Li_2S electrode, a significant portion of each particle is electrically isolated and can be oxidized at the localized interface between the electrode/electrolyte with sufficient charge transfer[7]; therefore, the Li_2S exhibits a large overpotential and a limited reversible capacity that is substantially lower than the theoretical value.[8] Furthermore, the dissolution-precipitation process yields insulating deposits of S and Li_2S, which passivate the active interface for the redox reaction.[9] Such evolution of the electrode architecture recurring over cycling is thus considered one of the primary causes of capacity fading in Li-S batteries together with internal polysulfide shuttling.[10,11] Consequently, Li-S cells have been shown to have insufficient practical energy density, poor rate capability, and limited cycle life, collectively restricting commercial success of this system.

Context & Scale

Li-S batteries have attracted considerable attention because of the natural abundance of sulfur and the high theoretical energy of 2,500 Wh kg^{-1}. This is enabled by the reversible conversion reaction between sulfur and Li_2S via a series of lithium polysulfide intermediates. The poor electronic conductivity of Li_2S imposes a large impedance in the cells and the dissolution-precipitation process yields insulating deposits of S and Li_2S. Herein, we introduce a new quinone-based redox mediator to facilitate Li_2S oxidation. Given the tailored properties of quinone molecules (redox potential, solubility, and electrochemical stability), the initial charging of Li_2S electrodes can occur below 2.5 V at a 0.5C rate for the first time and the subsequent discharge capacity is as high as 1,300 mAh g_s^{-1}. Moreover, randomly deposited dead Li_2S is effectively prevented, avoiding the primary cause of performance degradation in Li-S batteries upon cycling.

To address the aforementioned issues, considerable efforts have focused on incorporating nanostructured conductors, such as transition metals (Fe, Cu, and Co),[12–15] metal oxides,[16,17] metal sulfides,[18–20] metal nitrides,[21,22] metal carbides,[23] carbon nanomaterials,[24–29] and conductive polymers.[30] The electrochemically active area in the electrode significantly improved through these approaches, and LiPSs diffusion was further suppressed when appropriate physical confinement was attained. However, this improvement was often accomplished at the expense of the tap density with low active material loadings and would require costly production processes. Also, this approach does not necessarily prevent detachment of active particles from a conductive support and passivation of redox active sites upon long-term cycling during the solid-liquid-solid transition. Employing chemical interactions between LiPSs and hosts can better trap the sulfur species,[31–33] but this effect is specific to the host surfaces, raising concerns about the practical viability of requiring an ultrahigh-surface-area matrix. Therefore, breakthroughs are still needed to develop a low cost, scalable, and reliable method to improve the practical performance of Li-S batteries.

Introducing redox mediators (RMs) to the electrolyte solution represents another effective strategy to address the limited performance of Li-S batteries.[34] This approach relies on electrochemical oxidation of RMs in solution, which can in turn chemically oxidize the active material on the entire surface of the particle. This additional charge transfer route beyond the localized interface enables homogeneous and complete oxidation of the electrode with a reduced overpotential. This approach has been primarily explored in lithium-oxygen (Li-O_2) batteries, which suffer from the poor electronic conductivity of Li_2O_2.[35] Properly designed RMs have been shown to reduce the charge overpotential of Li_2O_2 by less than 0.1 V and protect both the electrolyte and carbon electrodes from degradation, significantly improving the energy efficiency and cycling stability of Li-O_2 cells.[36–38] In contrast, the research in utilizing RMs in Li-S batteries is still in its infancy. Soluble LiPSs are known to serve as an internal RM if available, but their transient nature renders LiPSs unreliable in the cell at fully discharged or charged states.[39] So far, only metallocene has been confirmed to shuttle electrons during Li_2S oxidation, which can reduce the initial charge potential of Li_2S electrodes to 2.9 V.[40] Lithium iodide (LiI) was also reported to reduce the polarization, but later it was found that it actually modified Li_2S surfaces; regardless, the charging occurs at 2.8 V, which still deviates from the Li_2S equilibrium potential.[41] Hence, the lack of proper redox chemistry has hindered the potential of employing RMs in Li-S batteries when compared to Li-O_2 batteries.

Here, we utilize quinone redox chemistry to design a new RM for fast and stable cycling of Li-S batteries. Through rational tuning of the redox potential, stability, and solubility of quinones by molecular engineering, we successfully demonstrated that the quinone redox can facilitate the initial oxidation of Li_2S below 2.5 V at a fast rate of 0.5C. The continuing effectiveness of the quinone-based RM beyond the first cycle was confirmed with the observation of minimal polarization and improved capacity retention of Li-S cells over prolonged cycles. Importantly, when cycled with the RM, the Li_2S electrode maintained its original morphology over 250 cycles, suggesting a unique mechanism that enables controlled deposition of Li_2S and sulfur instead of random deposition. Thus, minimal overpotential and high capacity continued over prolonged cycling. Because of these collective attributes, a high mass loading electrode of 6 mg cm^{-2} Li_2S was used to successfully demonstrate charging below 2.5 V with a reversible capacity of 952 mAh g_s^{-1}. This simple and effective strategy of using tailored RMs in sulfur redox chemistry to improve both

[1]Department of Chemistry, Stanford University, Stanford, CA 94305, USA

[2]Department of Chemical Engineering, Stanford University, Stanford, CA 94305, USA

[3]Stanford Synchrotron Radiation Lightsource, SLAC National Accelerator Laboratory, Menlo Park, CA 94025, USA

[4]Materials Sciences Division, Lawrence Berkeley National Laboratory, Berkeley, CA 94720, USA

[5]Performance Materials Technology Center, Corporate Research and Development, Asahi Kasei Corporation, 2-1 Samejima, Fuji, Shizuoka 416-8501, Japan

[6]Department of Materials Science and Engineering, Stanford University, Stanford, CA 94305, USA

[7]These authors contributed equally

[8]Lead Contact

*Correspondence: yicui@stanford.edu (Y.C.), zbao@stanford.edu (Z.B.)

https://doi.org/10.1016/j.joule.2018.12.018

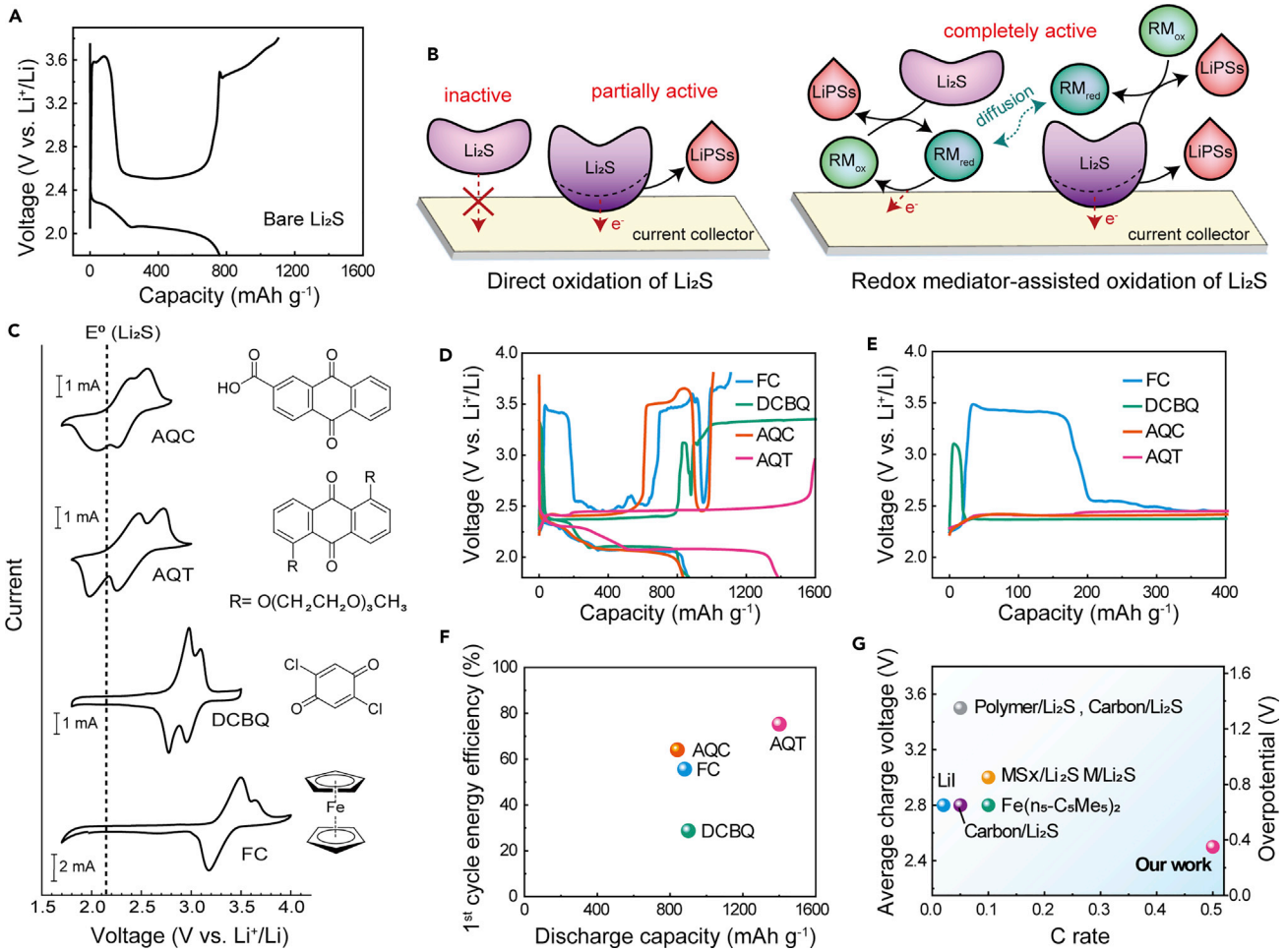

Figure 1. Tailored RMs to Facilitate Li_2S Oxidation

(A) A typical voltage profile of a bare Li_2S electrode in the first cycle at 0.3C. The charge cut-off voltage is 3.8 V.

(B) A schematic illustrating direct Li_2S oxidation and RM-assisted Li_2S oxidation in Li-S batteries.

(C) Cyclic voltammograms of different RMs (20 mM) in DOL/DME electrolyte and their chemical structures.

(D) Voltage profiles of Li_2S electrodes in the first cycle with different RMs at 0.3C. The same RM concentration (80 mM), Li_2S mass loading (0.7 mg cm^{-1}), and electrolyte to Li_2S ratio (28 μL mg^{-1}) were used as the baseline condition for the comparison (Li_2S:AQT molar ratio = 10:1).

(E) Enlarged charge voltage profiles from (D) to compare voltage overshoots.

(F) Comparison of different RM effects in the first cycle energy efficiency and discharge capacity of Li_2S electrodes.

(G) Average charge voltage and applied C rate in the first cycle demonstrated in previous studies and our work.

reaction kinetics and stability is the key to obtaining high practical power and energy density over prolonged cycling for the practical implementation of Li-S batteries.

RESULTS AND DISCUSSION

Large Overpotentials for Li_2S Cathodes

Due to poor electronic conductivity, Li_2S electrodes are difficult to activate. The oxidation reaction only occurs at the localized regions of the active particles directly interfacing electron and ion transfer channels. This mechanism thus requires a large overpotential, and the cell exhibits a specific capacity much lower than the theoretical value. Figure 1A shows the typical voltage profile of a Li_2S electrode in the first cycle at 0.3C using monodispersed microparticles (μ-Li_2S, 1.26 μm average diameter) (Figure S1), and the conventional electrolyte for Li-S batteries (i.e., 1 M lithium bis[trifluoromethanesulfonyl] imide in dioxolane/dimethoxyethane [DOL/DME] with

2 wt % $LiNO_3$). The electrolyte to Li_2S ratio was 28 μL mg^{-1}, which should be considered a flooded electrolyte condition. Upon charging, an overshoot as high as 3.6 V followed by a quick voltage drop to 2.6 V, then a high charge potential over 3.6 V, was observed. A high charge cut-off voltage of 3.8 V, which exceeds the stability limit of ethereal electrolytes, was applied in an attempt to further activate Li_2S; however, the discharge capacity was still less than 800 mAh g_s^{-1}, indicating less than 50% sulfur utilization. At a lower rate of 0.1C, the overpotential was reduced, permitting a lower charge cut-off voltage of 3.0 V (Figure S2); however, the discharge capacity remained insufficiently low, indicating a substantial amount of inactive Li_2S (52% sulfur utilization).

Design Rationales of the RM for Li_2S Cathodes

Effective RMs solubilized in the electrolyte shuttle electrons between current collectors and the surfaces of isolated Li_2S particles, which would have otherwise remained inactive (Figure 1B). During charging, the oxidized RMs with a redox potential higher than that of Li_2S can chemically oxidize Li_2S over the entire surface interfacing with the electrolyte and diffuse to current collectors where they are then electrochemically re-oxidized. Consequently, the charge voltage reflects the redox potential of the RM. Thus, the ideal redox potential of RMs would be slightly higher than the equilibrium potential of Li_2S (~2.15 V versus Li^+/Li) to minimize the hysteresis between charging and discharging in order to maximize energy efficiency. However, RMs in literature, including ferrocene (FC) and decamethylferrocene exhibit significantly higher redox potentials at 3.4 V and 2.9 V versus Li^+/Li, respectively. To design RMs with better matched redox potentials, we adopt the redox activity of quinones. The redox potentials of quinone molecules range from 1.7 V to 3.2 V versus Li^+/Li depending on the molecular structure. We rationalized that anthraquinone (AQ) derivatives would possess lower redox potential than benzoquinone (BQ) derivatives due to the electron-rich benzene rings. Then, we tailored the molecular structure of AQ to control the solubility in DOL/DME electrolyte and stability to maximize RM efficiency.

We first selected anthraquinone-2-carboxylic acid (AQC) and 2,5-dichloro-1,4-benzoquinone (DCBQ) as RMs to examine electrochemical properties. Figure 1C presents cyclic voltammograms (CVs) of the RMs versus lithium metal in the DOL/DME electrolyte. When compared with FC, quinone derivatives showed more favorable redox potentials that are better matched to that of Li_2S oxidation. In particular, AQC is preferred to facilitate Li_2S oxidation with minimal polarization. However, with continued cycling, we noticed that AQC had limited electrochemical stability in the operating condition of Li-S cells (Figure S3). Moreover, AQC had limited solubility (<20 mM) in the DOL/DME electrolyte, further limiting the usable RM quantity in the cell. In pursuit of designing a better RM, we introduced polar substituents (triethylene glycol monomethyl ether) to the AQ center to yield 1,5-bis(2-(2-(2-methoxyethoxy)ethoxy)ethoxy) anthra-9,10-quinone (AQT), which exhibits similar redox potentials to AQC (Figure 1C). AQT showed improved solubility (>500 mM) and markedly improved cycling stability compared to AQC, rendering the molecule more reliable as an RM.

The first cycle voltage profiles of Li_2S electrodes with different RMs at 0.3C are shown in Figure 1D. The same electrode and electrolyte condition used in Figure 1A was employed for the following comparative study except that 80 mM of RM was added to the electrolyte. The molar ratio of Li_2S to RM was fixed to 10:1. In accordance with our design rationales, AQT demonstrated exceptional performances when compared to other RMs. While the addition of both AQC and AQT prevents the

initial overshoot upon charging, only AQT can oxidize Li_2S at a constant potential below 2.5 V throughout the charging process. Remarkably, the cell with AQT exhibited much higher discharge capacity of 1,402 mAh g_s^{-1}, corresponding to 85% sulfur utilization, than the cell with AQC. Even under the condition where AQC and AQT were both fully soluble (20 mM, Figure S4), the cell with AQT showed a higher discharge capacity (810 mAh g_s^{-1}) than that with AQC (482 mAh g_s^{-1}), which may be due to the deteriorating stability of AQC during regeneration. On the other hand, DCBQ and FC showed limited improvement in promoting Li_2S oxidation, as expected, since their redox potentials are significantly higher than 2.1 V. The initial voltage overshoot decreased but remained above 3.0 V and 3.4 V for DCBQ and FC, respectively, which is consistent with their redox potentials (Figure 1E). Once LiPSs were formed and available as the additional RM in the electrolyte, the voltage dropped to 2.6 V. As LiPSs were exhausted, the voltage rose back to the redox potential of DCBQ and FC, respectively, which was then followed by another dip in the profile by forming additional LiPSs. Given this insufficient activation of the Li_2S electrode, the resulting discharge capacity did not improve considerably in either system when compared to the cell without RM.

We summarize the energy efficiency and discharge capacity of the various RMs in Figure 1F. Low polarization and high Coulombic efficiency lead to high energy efficiency. The Li_2S cell with AQT showed the highest discharge capacity (1,402 mAh g_S^{-1}), lowest average charge potential (<2.5 V), and highest Coulombic efficiency (87%), thus exhibiting the highest energy efficiency among all tested RMs. Taken together, AQT with the desired redox potential, high solubility in the electrolyte, and superior cycling stability is the most effective in promoting charge transport of Li_2S cathodes among all the tested systems.

With 10 mM of AQT in the electrolyte, where the molar ratio between Li_2S and AQT is 80 to 1, the overpotential during the first charging cycle can be effectively reduced Figure S5. Nevertheless, as the AQT concentration increases, the reversible capacity and Coulombic efficiency increase. Thus, we used either 80 mM or 160 mM of AQT depending on the electrode mass loading in the following study to assure improved performance. When we also decreased the electrolyte amount from 20 μL to 10 μL, which corresponds to the electrolyte/Li_2S of 14 μL mg^{-1}, the Li_2S electrode can be still charged at 2.5 V (Figure S6). Note that redox cycling of quinone is also effective in oxidizing ball-milled commercial Li_2S with a more heterogeneous size distribution than the μ-Li_2S (Figure S7).

Notably, AQT performs better than Li_2S_8, the internal RM spontaneously formed during conventional sulfur redox processes (Figure S8). When adding 80 mM Li_2S_8 as an RM to the DOL/DME electrolyte, the charge capacity obtained below 2.5 V is less than 400 mAh g_S^{-1} at 0.3C, which is 3-fold less than AQT. This result confirmed the need for an RM better than Li_2S_8 to minimize polarization during charging.

Next, we compared the maximum C rate achieved with various reported strategies using Li_2S electrodes and the corresponding first average charging voltage (Figure 1G). Methods such as mixing Li_2S with nanostructured conductors like carbon,[27,42–44] metals sulfides,[20,45] and polymers[25] still exhibit oxidation potentials of 2.8 V, 3.3 V, and 3.5 V, respectively, even at a slow rate (<0.1C), simultaneously suffering from process complexity and lower active material loadings. Likewise, the previous best-performing additives LiI and FC exhibited first charge potentials of 2.8 V at 0.05C and 2.9 V at 0.2C, respectively,[40,41] which are far above the equilibrium potential of Li_2S. In comparison, AQT can facilitate Li_2S oxidation at voltages

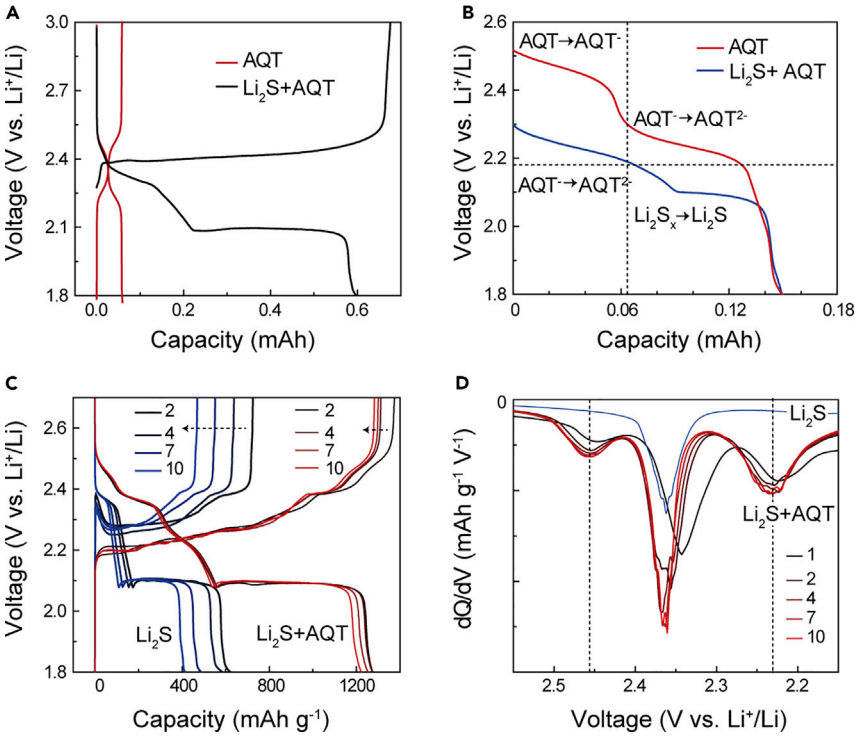

Figure 2. Chemical Reaction between AQT and Li_2S and the Resulting Electrochemistry

(A) Voltage profiles of half-cells using 80 mM AQT in DOL/DME electrolyte (20 μL) with and without a Li_2S electrode.

(B) Galvanostatic discharge profile of a half-cell with a Li_2S and 160 mM AQT mixture compared with the cell without Li_2S and only with 160 mM AQT.

(C and D) Voltage profiles of Li_2S electrode (0.7 mg cm^{-2}) cycled with and without AQT (80 mM) in the electrolyte (20 μL) (C) and corresponding dQ/dV curves at 0.1C (D).

as low as 2.45 V even at a high current density of 0.5C (Figure S9), which demonstrated that this system has exceptionally fast charge-transfer kinetics. The performance comparison is more reasonable when the critical cell parameters, including areal mass loading, active content, and electrolyte/active ratio, are considered in parallel. Thus, additional experimental conditions are listed in Table S1 for a detailed comparison. Note that the charge overpotential and the subsequent discharge capacity in our study are remarkable despite using large particles, a high active content, and a comparable electrolyte to Li_2S ratio.

Chemical Reaction between AQT and Li_2S

Figure 2A compares the voltage profiles of half-cells using 80 mM AQT in DOL/DME electrolyte (20 μL) with and without a Li_2S electrode, which exhibits capacities of 0.612 mAh and 0.059 mAh, respectively. Given that the charge voltage of the Li_2S electrode overlaps with the voltage range of AQT at 2.4 V, the charge process should involve the direct electrochemical oxidation of AQT. In the galvanotactic discharge and charge of AQT (as a catholyte), we confirmed stable reduction and oxidation of AQT with 80% capacity retention over 200 cycles and negligible redox shuttling of AQT with Coulombic efficiency higher than 98% throughout cycling (Figure S10). This result validates that AQT can continuously be reduced and oxidized in the presence of a lithium metal anode without significant degradation of the RM on the Li metal surface.

The spontaneous chemical reaction of Li_2S oxidation by AQT was investigated by X-ray photoelectron spectroscopy (XPS) (Figure S11). To probe changes in the oxidation state of Li_2S when mixed with AQT in its oxidized state, we measured the S2p binding energy of the Li_2S and AQT mixture (5:1 molar ratio) in the DOL/DME solvent. The result was compared to that of blank Li_2S and chemically synthesized Li_2S_4. The S2p spectrum of Li_2S_4 shows two pairs of doublets at 161.20/162.4 eV and 162.8/163.9 eV, which correspond to the terminal (S_T^{-1}) and bridge (S_B^0) S atoms, respectively,[46] in addition to minor contributions from the unreacted Li_2S at 159.67.20/160.85 eV. Similarly, the mixture of Li_2S and AQT exhibited significant contribution at higher S2p binding energies than pristine Li_2S. This arises from the oxidation of Li_2S by AQT, and thus proves the spontaneous charge transfer between Li_2S and AQT.

We could better understand the spontaneous chemical reaction of Li_2S oxidation by AQT by analyzing the reaction product. Since the reaction product simultaneously forms when we mix the Li_2S electrode and the AQT-containing electrolyte to fabricate the half-cell, we are thus able to electrochemically analyze the product by directly discharging the half-cell. Figure 2B shows the discharge profile of the half-cell with a mixture of Li_2S and 160 mM AQT, and it was compared with the cell without Li_2S and only having 160 mM AQT. Note that no discharge capacity would be exhibited when directly discharging pristine Li_2S. From the mixture, on the other hand, we observed a plateau at 2.25 V corresponding to the electrochemical reduction of the AQT^-, followed by a plateau at 2.1 V corresponding to the electrochemical reduction of Li_2S_x. Since the profile does not show the first reduction plateau of AQT at 2.45 V, it is confirmed that all of the AQT has been chemically converted into AQT^- when mixed with Li_2S. Simultaneously, chemical oxidation of Li_2S into Li_2S_x should occur. The discharge capacity is identical to that of pure AQT, indicating that the total amount of charge is retained and no side reaction occurs other than this process.

Further evidence of the charge transfer process between AQT and Li_2S was obtained with cyclic voltammetry. We conducted a cathodic sweep followed by an anodic sweep of AQT in DOL/DME electrolyte while gradually adding Li_2S_4 (Figure S12). The second oxidation peak at 2.6 V (O2) showed significant current responses upon addition of Li_2S_4, while the first oxidation peak (O1) showed negligible changes. This result indicates that the concentration of AQT^- to be oxidized at 2.6 V increases as the polysulfide concentration in the electrolyte increases due to the chemical regeneration of AQT^- from AQT.[47] We hypothesize that the chemical regeneration of AQ^- from AQ is promoted by Li_2S_x ($x < 4$), which can be formed during the previous cathodic sweep by reducing Li_2S_4 (for details, see Note S1).

Universal Improvement in Sulfur Electrochemistry by AQT

The effectiveness of AQT to improve the Li-S battery operation beyond the first cycle was confirmed over continued cycling (Figure 2C). During 10 cycles at 0.1C, the blank Li_2S electrode showed repeated overshooting in the initial stage of charging and the capacity continuously decreased to 400 mAh g_s^{-1}. In contrast, with AQT, no voltage overshoot was observed during charging, and 96% of the capacity at the second cycle was retained in the 10th cycle. Figure 2D depicts the differential capacity versus voltage (dQ/dV) obtained from the discharge profiles in Figure 2C. The enlarged dQ/dV curves displayed two consistent reduction peaks from AQT over 10 cycles, which were not observed in the pristine Li_2S cell, showing continuous redox activity of AQT over prolonged cycling.

To validate the effect of AQT to promote the sulfur electrochemistry generally, we fabricated cells using a Li_2S_8 catholyte instead of a Li_2S electrode. Figure S13A shows the voltage profiles of Li_2S_8 cells with and without AQT at 0.1C. The cells were first discharged to reduce Li_2S_8 to Li_2S and comparable capacities were obtained regardless of the AQT presence because pristine AQT does not participate in the reduction of Li_2S_8. Then, the cell charging with AQT showed a slightly lower overpotential when compared to the blank cell, and the subsequent discharge capacity was much higher in the presence of AQT. Note that the increased capacity (307 mAh g_s^{-1}) in the second cycle cannot fully account for the capacity contribution from AQT indicating more Li_2S can be activated with AQT in the Li_2S_8 catholyte cells as well. Upon prolonged cycling, the effect of AQT became prominent. Figure S13B presents the average charge and discharge voltage of the Li_2S_8 catholyte cells with AQT at rates of 0.1C, 0.3C, and 0.5C in comparison to the blank Li_2S_8 cell at 0.1C. The reduced polarization by AQT remarkably persisted over 200 cycles, demonstrating consistent charge transport kinetics over many cycles, outperforming the blank cells.

Improved Cycling Stability of Li-S Batteries by AQT

Another important feature is that adding AQT significantly enhances the cycling stability of Li-S batteries. As shown in Figure 3A, at a current density of 1C, the capacity of 850 mAh g_s^{-1} was retained after 500 cycles in the presence of AQT, whereas the capacity of the bare Li_2S cell decayed drastically to 225 mAh g_s^{-1} within 10 cycles (Figure 3A). At a lower rate of 0.5C, the capacity retention was still considerably better with AQT (Figure S14). This cycling stability is exceptional because it was achieved without specialized processing such as confinement or encapsulation of the sulfur species. The energy efficiency and Coulombic efficiency is also improved by adding AQT (Figure 3B). It is also important to note that AQT does not accelerate the self-discharge of Li-S batteries, but it prevents the capacity decrease due to the sulfur loss in later cycles (Figures S15 and S16), suggesting that shuttling of RM to the Li metal anode is negligible.

The capacity decay of Li-S batteries is attributed to the loss of active material due to the soluble intermediates and the propagation of the electrochemically inactive portion by pulverization and random deposition of insulating species during cycling. Therefore, to understand the origin of the improved cycle life with AQT, we explored the effects of AQT on both polysulfide dissolution and Li_2S morphology evolution.

First, we examined the solubility of representative LiPS species (Li_2S_4 and Li_2S_8) in DOL/DME upon AQT introduction. Polysulfide solutions (20 mM) were prepared as references, and an equivalent molar amount of AQT was added to the polysulfide solutions to prepare the mixtures. After filtering the solution to remove any particles, inductively coupled plasma optical emission spectrometry (ICP-OES) was used to quantify the total concentration of sulfur and lithium in the liquid phase. As shown in Figure 3C, the Li_2S_4 and AQT mixture contained only 25% of the expected sulfur content from the original pristine Li_2S_4 solution, and the Li_2S_8 and AQT mixture also contained less than 55% of the sulfur content from the pristine Li_2S_8 solution. Therefore, introducing AQT decreased the amount of soluble sulfur species in the electrolyte. We attributed the decreased LiPSs solubility to the binding interaction between AQT and LiPSs[48] (for details see Figure S17; Note S2).

Next, the morphology evolution of Li_2S electrodes over many cycles was monitored. The Li_2S electrodes tested with and without AQT were retrieved after the first and 250th cycles, respectively, (S18) and examined by scanning electron microscopy

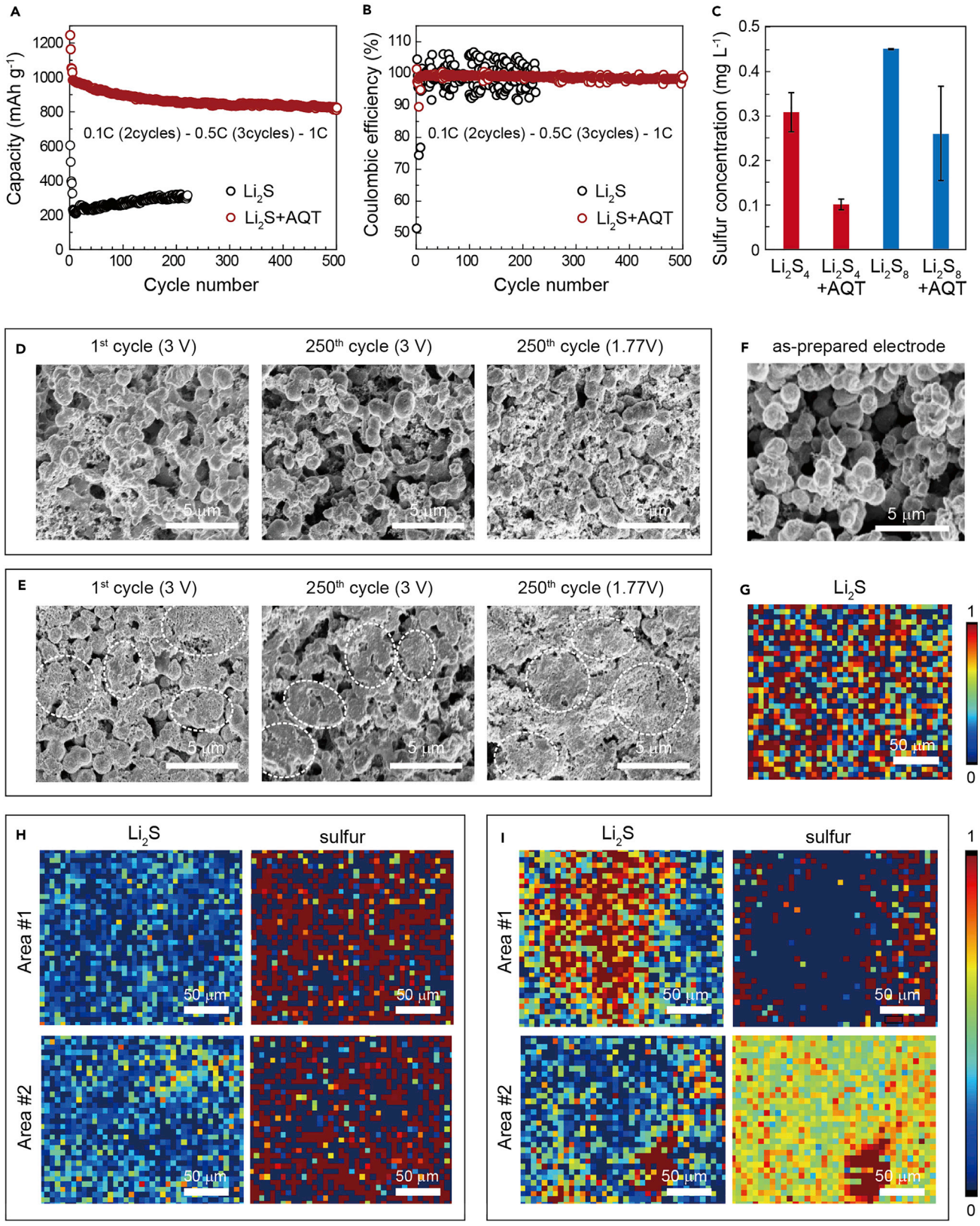
A
Capacity (mAh g-1)
Cycle number
0.1C (2cycles) - 0.5C (3cycles) - 1C
Li2S
Li2S+AQT
B
Coulombic efficiency (%)
Cycle number
0.1C (2cycles) - 0.5C (3cycles) - 1C
Li2S
Li2S+AQT
C
Sulfur concentration (mg L-1)
Li2S4
Li2S4 +AQT
Li2S8
Li2S8 +AQT
D
1st cycle (3 V)
250th cycle (3 V)
250th cycle (1.77V)
5 μm
E
1st cycle (3 V)
250th cycle (3 V)
250th cycle (1.77V)
5 μm
F
as-prepared electrode
5 μm
G
Li2S
50 μm
1
0
H
Li2S
sulfur
Area #1
Area #2
50 μm
I
Li2S
sulfur
Area #1
Area #2
50 μm
1
0

Figure 3. Improved Cycling Stability of Li_2S Electrode by AQT

(A and B) Capacity retention (A) and Coulombic efficiency (B) of Li_2S electrodes (0.7 mg cm^{-2}) cycled with and without AQT. The cells were first tested at 0.1C (2 cycles), then at 0.5C (3 cycles), and followed by continued cycling at 1C. The electrolyte to Li_2S ratio was 28 μL mg^{-1}.

(C) The solubility change of polysulfide intermediates in DOL/DME by adding AQT determined by ICP-OES.

(D–F) SEM images of cycled Li_2S electrodes with AQT (D) and without AQT (E) in the electrolyte. The predominant feature of unevenly deposited sulfur/Li_2S is indicated with the white circle. (F) The as-prepared electrode is shown for comparison.

(G–I) X-ray spectromicroscopy maps of the as-prepared Li_2S electrodes (G) and the cycled electrode in the charged state after 200 cycles with AQT (H) and without AQT (I) in the electrolyte.

(SEM) as shown in Figures 3D and 3E. The as-prepared electrode of Li_2S morphology is shown in Figure 3F. In accordance with the previous study under the conventional condition suffering from the recurring solid-liquid-solid transition,[11,16] randomly deposited sulfur species that are different from the initial morphology were observed in the blank Li_2S electrode regardless of the cycle number and state of the charge (Figure 3E). Such uneven accumulation of thick sulfur/Li_2S layers observed in SEM would block the charge transfer across the electrode/electrolyte interfaces and thus cause poor reaction kinetics and capacity decay. Nevertheless, in the presence of AQT, the original morphology of Li_2S particles was virtually unchanged over 250 cycles (Figure 3D). We observed such a phenomenon consistently from multiple spots over the entire electrode (Figures S19–S21). This controlled deposition of the solid species was identified as a critical feature to achieve long-term cycling to maintain the efficient charge transfer kinetics of the original porous electrodes throughout the operation.[16,49] The consistent morphology over prolonged cycling that accompanies the repeated solid-liquid-solid transition between Li_2S and S cannot be fully accounted for by the homogeneous oxidation over the Li_2S surface in the presence of AQT. We hypothesize that AQT can potentially alter LiPS-solvent interactions and determine sulfur speciation, as evidenced by the reduced solubility of LiPS with AQT, which in turn induces preferred deposition of Li_2S and S on the surfaces of active particles.

We further conducted *ex situ* X-ray spectromicroscopy with the Li_2S electrodes in the charged state that had been cycled over 200 times (Figure S22). The maps were collected at multiple spots on each sample (as indicated with area #1 and #2) at energies of 2,470.8, 2,472.6, 2,473.6, and 2,476.4 eV, in order to differentiate between Li_2S, polysulfide, and elemental sulfur species (Figure S23). First, the Li_2S map of the as-prepared electrode is shown in Figure 3G. After cycling for 200 times in the presence of AQT, the fully charged electrode showed a homogeneous sulfur distribution and a trace of Li_2S throughout the electrode (Figure 3H). In sharp contrast, when cycled without AQT, the Li_2S electrode displayed a localized region of sulfur with exceptionally high intensity (6–40 times higher than other regions) in the elemental sulfur map while also showing significant intensities from unreacted Li_2S in the Li_2S map (Figure 3I). This is consistent with our SEM result showing the heterogeneous conversion of sulfur during cycling. Thus, the results verify homogenous and complete conversion of sulfur over the entire electrode in the presence of AQT, which is highly desirable for improved energy density and cycle life. Due to the complex nature of sulfur speciation, further studies are needed to specify the sulfur redox mechanism with AQT by real-time monitoring of chemical and structural evolution of the electrode.

Outstanding Battery Performance with High Mass Loading

The above results suggest that AQT may effectively resolve poor charge transfer and heterogeneity in high mass loading electrodes. We tested thick Li_2S electrodes with areal Li_2S loading of 4 and 6 mg cm^{-2} in the presence of AQT. As shown in Figure S24, the first charge plateau remained below 2.6 V at 0.05C throughout the

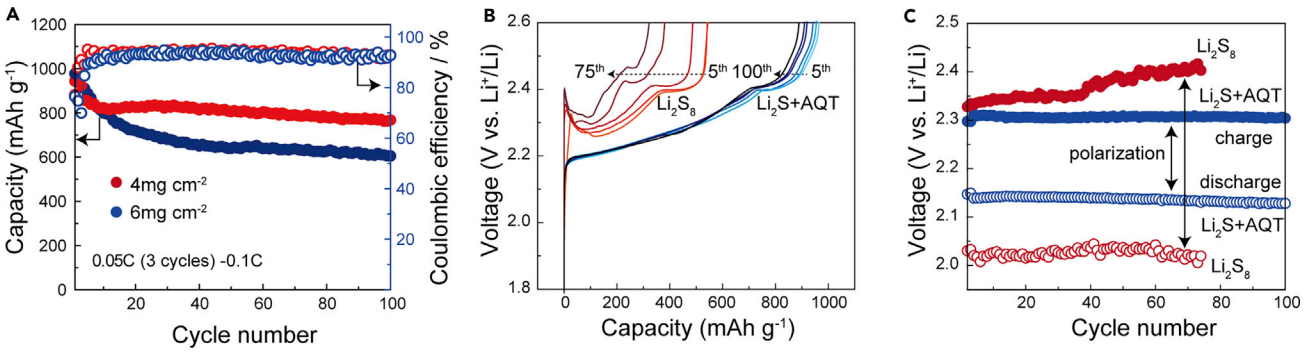

Figure 4. Electrochemical Performance of High Mass Loading Li_2S with AQT

(A) Capacity retention and Coulombic efficiency of high mass loading Li_2S cathodes (4 mg cm^{-2} and 6 mg cm^{-2}) using an electrolyte to Li_2S ratio of 12.5 μL mg^{-1}. The cells were initially tested at 0.05C for 3 cycles and then tested at 0.1C for the long-term cycling.

(B and C) Voltage profile evolution (B) and corresponding average charge and discharge voltages (C) over 100 cycles of the high mass loading electrodes. The performance of Li_2S cathode cycled with AQT is compared with that of Li_2S_8 catholyte with the equivalent sulfur loading (70% active, 3 mg cm^{-2}) at 0.1C.

charging process, and more than 950 mAh g_s^{-1} of discharge capacity was obtained in both electrodes. This supports our hypothesis that the redox mediating function of AQT effectively facilitates Li_2S oxidation even in thick electrodes with an electrolyte to Li_2S ratio of 12.5 μL m^{-1}. When cycled at 0.1C over 100 cycles, the 4 mg cm^{-2} electrode still exhibited a discharge capacity of 863 mAh g_s^{-1} with an average Coulombic efficiency of 93.7% and the 6 mg cm^{-2} electrode exhibited 606 mAh g_s^{-1} with an average Coulombic efficiency of 92.8% (Figure 4A). Notably, the above results were obtained by using μ-Li_2S (70 wt % of active content) without adopting any nanostructuring or hosts for the first time. This highlights the viability of using AQT as a simple and practical strategy to dramatically improve the performance of Li_2S electrodes for Li-S batteries. Nevertheless, when combined with optimized electrode architectures, further improvements in the performance and cell parameters (e.g., mass loading and electrolyte amount) would be feasible and would truly translate our fundamental discovery to real applications.[50,51]

We also confirmed that the charge transfer kinetics in the Li_2S cathode cycled with AQT is superior to that of the Li_2S_8 catholyte. Figure 4B compares multiple charge profiles over prolonged cycling of the Li_2S cathode with AQT against Li_2S_8 catholyte having the equivalent sulfur loading of 3 mg cm^{-2} and the active content of 70%. Surprisingly, we found that voltage profiles significantly evolved over time in the catholyte system whereas the profiles of the AQT-added Li_2S cathode remained unchanged for more than 100 cycles. When comparing the average voltage of charge and discharge curves over cycling for those two conditions (Figure 4C), reliably consistent and lower polarization was observed in the Li_2S electrode with AQT, highlighting stable and efficient sulfur redox cycling enabled by AQT.

Conclusion

We presented an effective strategy to facilitate Li_2S oxidation with minimal overpotential by using an anthraquinone redox center tethered with polyether chains, which exhibited the desired redox potential, high stability, and sufficient solubility in the electrolyte. Furthermore, we provided direct experimental evidence that AQT prevents polysulfide dissolution and preserves electrode morphology to ensure exceptional cycling stability. Collectively, the introduction of AQT as an RM is a simple and effective approach to significantly enhance multiple aspects of sulfur redox chemistry under challenging conditions. Unlike conventional approaches that often require

complicated nanofabrication, which inevitably increases battery costs, RMs can simply be added into the electrolyte and are thereby suitable for scalable production, enabling Li-S batteries as a viable technology.

EXPERIMENTAL PROCEDURES

Full details of the experimental procedures are provided in the Supplemental Information.

SUPPLEMENTAL INFORMATION

Supplemental Information includes 25 figures, 1 table, and 2 notes and can be found with this article online at https://doi.org/10.1016/j.joule.2018.12.018.

ACKNOWLEDGMENTS

This work is supported by the US Department of Energy, under the assistant Secretary for Energy Efficiency and Renewable Energy, Office of Vehicle Technologies, the Battery Materials Research (BMR) Program and Battery 500 Consortium, and the Joint Center for Energy Storage Research (JCESR). Use of the Stanford Synchrotron Radiation Lightsource, SLAC National Accelerator Laboratory, is supported by the US Department of Energy, Office of Science, Office of Basic Energy Sciences under Contract No. DE-AC02-76SF00515. The authors thank Sam Webb, Courtney Roach, and Erik Nelson for their assistance at BL 14-3. H.T. was supported by an appointment to the Intelligence Community Postdoctoral Research Fellowship Program at Stanford University, administered by Oak Ridge Institute for Science and Education through an interagency agreement between the US Department of Energy and the Office of the Director of National Intelligence.

AUTHOR CONTRIBUTIONS

Conceptualization, Y.T. and M.L.; Methodology, Y.T. and M.L.; Investigation, Y.T., M.L., E.C.M., G.G., S.C., T.K., H.T., and J.P.; Writing – Original Draft, M.L. and Y.T.; Writing – Review & Editing, M.L., Y.T., J.P, H.T., E.C.M., Y.C., and Z.B.; Funding Acquisition, Z.B. and Y.C.; Resources, E.C.M., L.W.W.; Supervision, Z.B. and Y.C.

DECLARATION OF INTERESTS

The authors declare no competing interests.

Received: July 13, 2018
Revised: September 28, 2018
Accepted: December 20, 2018
Published: January 22, 2019

REFERENCES

1. Bruce, P.G., Freunberger, S.A., Hardwick, L.J., and Tarascon, J.-M. (2012). Li–O_2 and Li–S batteries with high energy storage. Nat. Mater. *11*, 19–29.

2. Grey, C.P., and Tarascon, J.M. (2017). Sustainability and in situ monitoring in battery development. Nat. Mater. *16*, 45–56.

3. Pang, Q., Liang, X., Kwok, C.Y., and Nazar, L.F. (2016). Advances in lithium–sulfur batteries based on multifunctional cathodes and electrolytes. Nat. Energy *1*, 16132.

4. Wild, M., O'Neill, L., Zhang, T., Purkayastha, R., Minton, G., Marinescu, M., and Offer, G.J. (2015). Lithium sulfur batteries, a mechanistic review. Energy Environ. Sci. *8*, 3477–3494.

5. Yu, X., and Manthiram, A. (2017). Electrode–electrolyte interfaces in lithium–sulfur batteries with liquid or inorganic solid electrolytes. Acc. Chem. Res. *50*, 2653–2660.

6. Seh, Z.W., Sun, Y., Zhang, Q., and Cui, Y. (2016). Designing high-energy lithium-sulfur batteries. Chem. Soc. Rev. *45*, 5605–5634.

7. Lang, S.Y., Xiao, R.J., Gu, L., Guo, Y.G., Wen, R., and Wan, L.J. (2018). Interfacial mechanism in lithium–sulfur batteries: How salts mediate the structure evolution and dynamics. J. Am. Chem. Soc. *140*, 8147–8155.

8. Son, Y., Lee, J.-S., Son, Y., Jang, J.-H., and Cho, J. (2015). Recent advances in lithium sulfide cathode materials and their use in lithium sulfur batteries. Adv. Energy Mater. *5*, 1500110.

9. Fan, F.Y., Carter, W.C., and Chiang, Y.-M. (2015). Mechanism and kinetics of Li2S precipitation in lithium–sulfur batteries. Adv. Mater. *27*, 5203–5209.

10. Jin, Y., Zhou, G., Shi, F., Zhuo, D., Zhao, J., Liu, K., Liu, Y., Zu, C., Chen, W., Zhang, R., et al. (2017). Reactivation of dead sulfide species in

lithium polysulfide flow battery for grid scale energy storage. Nat. Commun. *8*, 462.

11. Yao, H., Zheng, G., Hsu, P., Kong, D., Cha, J.J., Li, W., Seh, Z.W., McDowell, M.T., Yan, K., Liang, Z., et al. (2014). Improving lithium–sulphur batteries through spatial control of sulphur species deposition on a hybrid electrode surface. Nat. Commun. *5*, 3943.

12. Hayashi, A., Ohtsubo, R., Ohtomo, T., Mizuno, F., and Tatsumisago, M. (2008). All-solid-state rechargeable lithium batteries with Li_2S as a positive electrode material. J. Power Sources *183*, 422–426.

13. Obrovac, M.N., and Dahn, J.R. (2002). Electrochemically active lithia/metal and lithium sulfide/metal composites. Electrochem. Solid State Lett. *5*, A70.

14. Sun, Y., Lee, H.-W., Seh, Z.W., Zheng, G., Sun, J., Li, Y., and Cui, Y. (2016). Lithium sulfide/metal nanocomposite as a high-capacity cathode prelithiation material. Adv. Energy Mater. *6*, 1600154.

15. Zhou, Y., Wu, C., Zhang, H., Wu, X., and Fu, Z. (2007). Electrochemical reactivity of Co–Li_2S nanocomposite for lithium-ion batteries. Electrochim. Acta *52*, 3130–3136.

16. Pang, Q., Kundu, D., Cuisinier, M., and Nazar, L.F. (2014). Surface-enhanced redox chemistry of polysulphides on a metallic and polar host for lithium-sulphur batteries. Nat. Commun. *5*, 4759.

17. Tao, X., Wang, J., Liu, C., Wang, H., Yao, H., Zheng, G., Seh, Z.W., Cai, Q., Li, W., Zhou, G., et al. (2016). Balancing surface adsorption and diffusion of lithium-polysulfides on nonconductive oxides for lithium-sulfur battery design. Nat. Commun. *7*, 11203.

18. Pang, Q., Kundu, D., and Nazar, L.F. (2015). A graphene-like metallic cathode host for long-life and high-loading lithium–sulfur batteries. Mater. Horiz. *3*, 130–136.

19. Yuan, Z., Peng, H.-J., Hou, T.-Z., Huang, J.-Q., Chen, C.-M., Wang, D.-W., Cheng, X.-B., Wei, F., and Zhang, Q. (2016). Powering lithium–sulfur battery performance by propelling polysulfide redox at sulfiphilic hosts. Nano Lett. *16*, 519–527.

20. Zhou, G., Tian, H., Jin, Y., Tao, X., Liu, B., Zhang, R., Seh, Z.W., Zhuo, D., Liu, Y., Sun, J., et al. (2017). Catalytic oxidation of Li2S on the surface of metal sulfides for Li- S batteries. Proc. Natl. Acad. Sci. USA *114*, 840–845.

21. Cui, Z., Zu, C., Zhou, W., Manthiram, A., and Goodenough, J.B. (2016). Mesoporous titanium nitride-enabled highly stable lithium-sulfur batteries. Adv. Mater. *28*, 6926–6931.

22. Sun, Z., Zhang, J., Yin, L., Hu, G., Fang, R., Cheng, H.-M., and Li, F. (2017). Conductive porous vanadium nitride/graphene composite as chemical anchor of polysulfides for lithium-sulfur batteries. Nat. Commun. *8*, 14627.

23. Liang, X., Garsuch, A., and Nazar, L.F. (2015). Sulfur cathodes based on conductive MXene nanosheets for high-performance lithium–sulfur batteries. Angew. Chem. Int. Ed. *54*, 3907–3911.

24. Fu, Y., Su, Y.-S., and Manthiram, A. (2014). Li_2S-carbon sandwiched electrodes with superior performance for lithium-sulfur batteries. Adv. Energy Mater. *4*, 1300655.

25. Guo, J., Yang, Z., Yu, Y., Abruña, H.D., and Archer, L.A. (2013). Lithium-sulfur battery cathode enabled by lithium-nitrile interaction. J. Am. Chem. Soc. *135*, 763–767.

26. Suo, L., Zhu, Y., Han, F., Gao, T., Luo, C., Fan, X., Hu, Y.-S., and Wang, C. (2015). Carbon cage encapsulating nano-cluster Li_2S by ionic liquid polymerization and pyrolysis for high performance Li–S batteries. Nano Energy *13*, 467–473.

27. Tan, G., Xu, R., Xing, Z., Yuan, Y., Lu, J., Wen, J., Liu, C., Ma, L., Zhan, C., Liu, Q., et al. (2017). Burning lithium in CS2 for high-performing compact Li_2S-graphene nanocapsules for Li–S batteries. Nat. Energy *2*, 17090.

28. Ji, X., Lee, K.T., and Nazar, L.F. (2009). A highly ordered nanostructured carbon–sulphur cathode for lithium–sulphur batteries. Nat. Mater. *8*, 500–506.

29. Song, M.-K., Zhang, Y., and Cairns, E.J. (2013). A long-life, high-rate lithium/sulfur cell: A multifaceted approach to enhancing cell performance. Nano Lett. *13*, 5891–5899.

30. Seh, Z.W., Wang, H., Hsu, P.-C., Zhang, Q., Li, W., Zheng, G., Yao, H., and Cui, Y. (2014). Facile synthesis of Li_2S-polypyrrole composite structures for high-performance Li_2S cathodes. Energy Environ. Sci. *7*, 672–676.

31. Pang, Q., and Nazar, L.F. (2016). Long-Life and high-areal-capacity Li–S batteries enabled by a light-weight polar host with intrinsic polysulfide adsorption. ACS Nano *10*, 4111–4118.

32. Demir-Cakan, R., Morcrette, M., Nouar, F., Davoisne, C., Devic, T., Gonbeau, D., Dominko, R., Serre, C., Férey, G., and Tarascon, J. (2011). Cathode composites for Li–S batteries via the use of oxygenated porous architectures. J. Am. Chem. Soc. *133*, 16154–16160.

33. Zheng, J., Tian, J., Wu, D., Gu, M., Xu, W., Wang, C., Gao, F., Engelhard, M.H., Zhang, J., Liu, J., et al. (2014). Lewis acid–base interactions between polysulfides and metal organic framework in lithium sulfur batteries. Nano Lett. *14*, 2345–2352.

34. Zhang, Z.-W., Peng, H.-J., Zhao, M., and Huang, J.-Q. (2018). Heterogeneous/homogeneous mediators for high-energy-density lithium–sulfur batteries: Progress and prospects. Adv. Funct. Mater. *28*, 1707536.

35. Park, J.-B., Lee, S.H., Jung, H.-G., Aurbach, D., and Sun, Y.-K. (2018). Redox mediators for Li–O_2 batteries: Status and perspectives. Adv. Mater. *30*, 1704162.

36. Gao, X., Chen, Y., Johnson, L.R., Jovanov, Z.P., and Bruce, P.G. (2017). A rechargeable lithium-oxygen battery with dual mediators stabilizing the carbon cathode. Nat. Energy *2*, 17118.

37. Lim, H.-D., Lee, B., Zheng, Y., Hong, J., Kim, J., Gwon, H., Ko, Y., Lee, M., Cho, K., and Kang, K. (2016). Rational design of redox mediators for advanced Li-O_2 batteries. Nat. Energy *1*, 16066.

38. Liu, T., Leskes, M., Yu, W., Moore, A.J., Zhou, L., Bayley, P.M., Kim, G., and Grey, C.P. (2015). Cycling Li-O_2 batteries via LiOH formation and decomposition. Science *350*, 530–533.

39. Yang, Y., Zheng, G., Misra, S., Nelson, J., Toney, M.F., and Cui, Y. (2012). High-capacity micrometer-sized Li_2S particles as cathode materials for advanced rechargeable lithium-ion batteries. J. Am. Chem. Soc. *134*, 15387–15394.

40. Meini, S., Elazari, R., Rosenman, A., Garsuch, A., and Aurbach, D. (2014). The use of redox mediators for enhancing utilization of Li_2S cathodes for advanced Li-S battery systems. J. Phys. Chem. Lett. *5*, 915–918.

41. Wu, F., Lee, J.T., Nitta, N., Kim, H., Borodin, O., and Yushin, G. (2015). Lithium iodide as a promising electrolyte additive for lithium-sulfur batteries: Mechanisms of performance enhancement. Adv. Mater. *27*, 101–108.

42. Dong, Y., Li, S., Zhao, K., Han, C., Chen, W., Wang, B., Wang, L., Xu, B., Wei, Q., Zhang, L., et al. (2015). Hierarchical zigzag $Na_{1.25}V_3O_8$ nanowires with topotactically encoded superior performance for sodium-ion battery cathodes. Energy Environ. Sci. *8*, 1267–1275.

43. Han, K., Shen, J., Hayner, C.M., Ye, H., Kung, M.C., and Kung, H.H. (2014). Li_2S-reduced graphene oxide nanocomposites as cathode material for lithium sulfur batteries. J. Power Sources *251*, 331–337.

44. Wu, M., Cui, Y., and Fu, Y. (2015). Li2S nanocrystals confined in free-standing carbon paper for high performance lithium–sulfur batteries. ACS Appl. Mater. Interfaces *7*, 21479–21486.

45. Seh, Z.W., Yu, J.H., Li, W., Hsu, P.-C., Wang, H., Sun, Y., Yao, H., Zhang, Q., and Cui, Y. (2014). Two-dimensional layered transition metal disulphides for effective encapsulation of high-capacity lithium sulphide cathodes. Nat. Commun. *5*, 5017.

46. Liang, X., Hart, C., Pang, Q., Garsuch, A., Weiss, T., and Nazar, L.F. (2015). A highly efficient polysulfide mediator for lithium-sulfur batteries. Nat. Commun. *6*, 5682.

47. Mogharrab, N., and Ghourchian, H. (2005). Anthraquinone 2-carboxylic acid as an electron shuttling mediator and attached electron relay for horseradish peroxidase. Electrochem. Commun. *7*, 466–471.

48. Li, G., Wang, X., Seo, M.H., Li, M., Ma, L., Yuan, Y., Wu, T., Yu, A., Wang, S., Lu, J., et al. (2018). Chemisorption of polysulfides through redox reactions with organic molecules for lithium–sulfur batteries. Nat. Commun. *9*, 705.

49. Pan, H., Chen, J., Cao, R., Murugesan, V., Rajput, N.N., Han, K.S., Persson, K., Estevez, L., Engelhard, M.H., Zhang, J., et al. (2017). Non-encapsulation approach for high-performance Li-S batteries through controlled nucleation and growth. Nat. Energy *2*, 813–820.

50. Chung, S.-H., and Manthiram, A. (2018). Designing lithium-sulfur cells with practically necessary parameters. Joule *2*, 710–724.

51. Chung, S.-H., Chang, C.-H., and Manthiram, A. (2018). Progress on the critical parameters for lithium-sulfur batteries to be practically viable. Adv. Funct. Mater. *28*, 1801188.